Original Article

Mitochondrial cholesterol metabolism related gene model predicts prognosis and treatment response in hepatocellular carcinoma

Xuna Guo[1#], Feng Wang[2#], Xuejing Li[3], Qiuqian Luo[3], Bihan Liu[1], Jianhui Yuan[1,3,4]

[1]Department of Biomedical Engineering, School of Life Sciences, Guangxi Medical University, Nanning, China; [2]Department of Biochemistry and Molecular Biology, School of Basic Medical Sciences, Guangxi Medical University, Nanning, China; [3]Department of Physiology, School of Basic Medical Sciences, Guangxi Medical University, Nanning, China; [4]Department of Physics, Guangxi Medical University, Nanning, China

Contributions: (I) Conception and design: X Guo, F Wang, J Yuan; (II) Administrative support: F Wang, J Yuan; (III) Provision of study materials or patients: None; (IV) Collection and assembly of data: Q Luo, B Liu; (V) Data analysis and interpretation: X Guo, X Li; (VI) Manuscript writing: All authors; (VII) Final approval of manuscript: All authors.

[#]These authors contributed equally to this work as co-first authors.

Correspondence to: Feng Wang, PhD. Department of Biochemistry and Molecular Biology, School of Basic Medical Sciences, Guangxi Medical University, 22 Shuangyong Road, Nanning 530021, China. Email: wangf@sr.gxmu.edu.cn; Jianhui Yuan, PhD. Department of Biomedical Engineering, School of Life Sciences, Guangxi Medical University, 22 Shuangyong Road, Nanning 530021, China; Department of Physiology, School of Basic Medical Sciences, Guangxi Medical University, Nanning, China; Department of Physics, Guangxi Medical University, Nanning, China. Email: yuanjianhui@gxmu.edu.cn.

Background: The persistently high mortality and morbidity rates of hepatocellular carcinoma (HCC) remain a global concern. Notably, the disruptions in mitochondrial cholesterol metabolism (MCM) play a pivotal role in the progression and development of HCC, underscoring the significance of this metabolic pathway in the disease's etiology. The purpose of this research was to investigate genes associated with MCM and develop a model for predicting the prognostic features of patients with HCC.

Methods: MCM-related genes (MCMGs) were identified through The Cancer Genome Atlas (TCGA), The Molecular Signatures Database (MsigDB), and the Mitocarta3.0 databases. Differential gene expression analysis and least absolute shrinkage and selection operator (LASSO) Cox regression analysis were performed using R software to construct a MCM-related model. This model underwent further analysis for somatic mutations, single sample gene set enrichment analysis (ssGSEA), stromal and immune cell estimation, immune checkpoint evaluation, and drug susceptibility prediction to assess the tumor microenvironment (TME) and therapeutic responses. The mRNA expression levels of the genes associated with the model were quantified using real-time fluorescence quantitative polymerase chain reaction (RT-qPCR).

Results: The model, which included six MCMGs (*ACADL*, *ACLY*, *TXNRD1*, *DTYMK*, *ACAT1*, and *FLAD1*), divided all patients (age ≤65 *vs.* >65 years, P<0.001; male *vs.* female, ns) into a high-risk group and a low-risk group. The high-risk group showed a higher mortality rate and lower survival rate with AUC of 0.785, 0.752, 0.756, 0.774 and 0.759 for the 1-, 2-, 3-, 4-, and 5-year respectively. A nomogram based on risk score, stage, T, and M had a better prognostic accuracy, with AUC of 0.808, 0.796, 0.811, 0.824 and 0.795 for the 1-, 2-, 3-, 4-, and 5-year respectively. The high-risk group showed enrichment in cell cycle, cell division, and chromosome processes, and a significantly higher tumor mutation burden (TMB) value compared to the low-risk group. Further immune infiltration analysis indicated a significantly reduction in the abundances of some immune cells (activated CD4 T cells, type 2 helper T cells, and neutrophils) and significantly higher expression levels of some immune checkpoint (*CD80*, *CTLA4*, *HAVCR2*, and *TNFRSF4*) in the high-risk group. Moreover, the risk score was associated with the response to immune checkpoint inhibitors (ICIs) therapy and efficiencies of multiple chemotherapy drugs.

Conclusions: This study developed a prognostic model based on MCMGs, which can predict the prognosis of liver cancer patients and their response to immunotherapy and chemotherapy. The model may provide new strategies to enhance the prognosis and treatment of HCC.

Introduction

In 2024, primary liver cancer accounted for approximately 41,630 new cases and 29,840 deaths, ranking it as the sixth most frequently diagnosed cancer and the third leading cause of cancer-related mortality globally (1). By 2040, it is projected that 1.3 million deaths will occur annually due to liver cancer, representing 56.4% of all cancer deaths (2). Among liver cancer cases, hepatocellular carcinoma (HCC) predominates comprising 75–85% of all instances, characterized by its insidious onset, multifarious etiology, and high mortality rate (3). Despite advancements in treatment modalities, including sorafenib chemotherapy, vascular catheterization, radiofrequency ablation, surgical resection, and liver transplantation, the recurrence rate

remains high, even among patients who undergo early treatment (4-6). Traditional prognostic models have been inadequate in achieving satisfactory outcomes due to the heterogeneity of HCC patients (7). Therefore, there is an urgent need to develop innovative and effective prognostic models that can accurately identify high-risk patients with poor prognosis, thereby enhancing the prognosis of HCC.

Alterations in mitochondrial cholesterol metabolism (MCM) significantly influence cancer cell biology by affecting mitochondrial function, metabolic reprogramming, apoptosis, and chemotherapy resistance (8). For instance, in rats with transplanted HCC, mitochondrial cholesterol levels were correlated with tumor growth and malignancy (9,10). Research indicates that maintaining homeostasis and regulating cholesterol metabolism within mitochondria are critical in various disease conditions (11). Therefore, it is imperative to investigate the molecular mechanisms underlying abnormal MCM in order to enhance the prognosis of HCC patients. In this study, a new prognostic model has been developed carefully, based on six MCMGs by utilizing gene expression data and clinical parameters. The predictive power of the model is rigorously evaluated on a range of key outcomes, including immunotherapy response, drug sensitivity, and immunoscape. We present this article in accordance with the TRIPOD reporting checklist (available at https://tcr.amegroups.com/article/view/10.21037/tcr-24-1153/rc).

Highlight box

Key findings

- The study developed a six-gene predictive model based on mitochondrial cholesterol metabolism-related genes (MCMGs), which effectively predicts the prognosis and treatment response of hepatocellular carcinoma (HCC) patients.
- The study found that the model can predict not only the survival rate of patients but also their response to immunotherapy and chemotherapy drugs.

What is known and what is new?

- MCMGs play an important role in various tumors.
- This study established and validated the risk model based on MCMGs.

What is the implication, and what should change now?

- This study developed a prognostic model for HCC based on MCMGs. The model's validity was confirmed through external datasets, demonstrating its predictive power. This research provides a new strategy for improving the prognosis and treatment of HCC patients. Currently, while abnormalities in mitochondrial cholesterol metabolism play a crucial role in HCC development, the clinical application value of MCMGs has not been systematically explored. Future research and clinical practice should pay more attention to MCMGs. This will significantly improve the prognosis of HCC patients, optimize treatment plans, and help develop a new therapeutic target and method.

Methods

Data collection and pretreatment

The Cancer Genome Atlas Liver Hepatocellular Carcinoma (TCGA-LIHC) (https://tcga-data.nci.nih.gov/tcga/) dataset was analyzed to obtain mRNA expression levels and clinical data for 365 HCC patients, serving as the training set. Data from the Gene Expression Omnibus (GEO) (https://www.ncbi.nlm.nih.gov/geo/) and the International Cancer Genome Consortium (ICGC) (https://icgc.org/) were employed to obtain

the GSE14520-GPL3921 and ICGC-LIRI-JP cohorts, respectively, which served as validation sets. Genes related to cholesterol metabolism and mitochondrial function were derived from the MitoCarta3.0 (http://www.broadinstitute.org/mitocarta) and the Molecular Signature Database (MsigDB: https://www.gsea-msigdb.org). The study was conducted in accordance with the Declaration of Helsinki (as revised in 2013).

Differentially expressed MCMGs

The analysis of differentially expressed genes (DEGs) was conducted utilizing the R package "DESeq2", with a stringent selection criterion of |log$_2$ fold change| >1 and adjusted P value <0.05, ensuring a robust identification of genes with significant expression variations. MCMGs were identified by comparing DEGs in HCC using a Venn diagram with genes associated with mitochondria and cholesterol metabolism (12).

Construction of a prognostic genes model

The Univariate Cox regression analysis (P<0.1) identified differentially expressed MCMGs with prognostic significance. The least absolute shrinkage and selection operator (LASSO) Cox regression analysis was then employed to establish a prognostic risk model, including the six most significant genes (*ACADL*, *ACLY*, *TXNRD1*, *DTYMK*, *ACAT1*, and *FLAD1*) (13). The risk score for the model was calculated as follows:

$$\text{Risk score} = \sum_{i=1}^{n} \text{expression}_{\text{genei}} \times \text{coefficients}_{\text{genei}} \quad [1]$$

HCC patients were classified into high-risk and low-risk groups based on their median risk score. Extensive clinical data from the TCGA database were used, and time-dependent receiver operating characteristic (ROC) analysis was performed using the "timeROC" and "survminer" R packages. Survival analysis was conducted on the high-risk and low-risk groups using the "survival" and "survminer" R packages. The effectiveness of the model was validated using the GSE14520 and ICGC datasets as external validation sets, with survival and time-dependent ROC analyses performed on these datasets.

Determination of independent prognostic parameters

The univariate and multivariate regression analyses were performed on risk scores and clinical characteristics including age, gender, grade, stage, and TNM to identify independent prognostic factors (P<0.05) (14).

Construction of a nomogram

Logistic regression analysis was utilized to construct a Cox risk model, which integrates risk scores and clinical variables. A predictive nomogram for HCC patients was constructed based on these parameters (15). Time-dependent ROC curves compared overall survival (OS) rates at various time points (P<0.05) (16). The concordance index (C-index) was used to assess the model ability to differentiate high-risk and low-risk patients.

Functional enrichment analysis and somatic mutation analysis in the high-risk and low-risk group

The "limma" R package was used to identify differentially expression genes between high-risk and low-risk groups. Pathway and function annotations were conducted using the "clusterProfiler" R package (17), with Gene Ontology (GO) and Kyoto Encyclopedia of Genes and Genomes (KEGG) enrichment studies. Gene set enrichment analysis (GSEA) revealed various biological pathways (18). Somatic mutation analysis was visualized using waterfall plots created with the "maftools" R package (19), providing insights into gene mutations and risk scores.

Immune infiltration analysis

Single-sample gene set enrichment analysis (ssGSEA) was conducted on 28 immune cell types in high-risk and low-risk groups, incorporating comparisons of 14 immunological checkpoints. Additionally, the Cell-type Identification By Estimating Relative Subsets Of RNA Transcripts (CIBERSORT) algorithm employed the model relationship with 22 immune cell types to explore their interaction within the immune landscape (20).

Immunotherapy efficacy prediction

The immunophenoscore (IPS) for HCC patients was acquired through The Cancer Imaging Archive (TCIA: https://tcia.at/home) online database, which employed machine learning technologies to calculate z-scores based on four cell types related to immunogenicity (21). The prognostic accuracy of the MCMGs model for

immunotherapy was performed using the iMvigor210 cohort (22).

Chemotherapeutic drug sensitivity analysis

The R packages "pRRophetic" and "ggplot2" predicted drug sensitivity in HCC patients by comparing the half-maximal inhibitory concentration (IC_{50}) values between high-risk and low-risk groups (23).

Cell culture and real-time fluorescence quantitative polymerase chain reaction (RT-qPCR)

Huh7 human HCC cells were purchased from the Cell Bank of the Chinese Academy of Sciences in Shanghai, China. Human normal hepatocytes THLE-2, human HCC HCCLM3 cells and human HepG2 cells were procured from the Laboratory of Biochemistry and Molecular Biology at Guangxi Medical University. The cells were cultured in DMEM high glucose complete media with 10% fetal bovine serum (FBS), 1% penicillin-streptomycin, and maintained at 37 ℃ with 5% CO_2. RNA extraction was carried out using a kit from Tiangen Biochemical Technology, and complementary DNA (cDNA) synthesis was conducted using the Transcriptor First Strand cDNA Synthesis Kit from Roche. RT-qPCR was conducted using PowerUp™ SYBR™ Green Master Mix from Thermo Fisher, with primer sequences listed in the Table S1. The $2^{-\Delta\Delta Ct}$ method was used to assess the relative expression levels of the target genes in each sample.

Statistical analysis

Data analysis was conducted using R software (version 4.1.0). Statistical significance of normally distribution variables was assessed using *t*-tests, whereas non-normally distributed variables were assessed using the Wilcoxon rank sum test (24). A significance threshold of $P<0.05$ was employed to ascertain statistical significance.

Results

Identification of MCMGs for HCC patients

The flowchart depicted the development of the MCMGs model, the prognostic evaluation, and various synthesized analyses (*Figure 1*). The screening criteria for identifying DEGs using the "Deseq2" R software were |$\log_2$

fold change|>1 and P<0.05 (*Figure 2A*). Through the intersection of DEGs with mitochondrial and cholesterol metabolism-related genes, 25 differentially expressed MCMGs were identified (*Figure 2B,2C*). Variations in the expression levels of these 25 genes between normal and tumor samples were illustrated using box plots (*Figure 2D*).

Construction and evaluation of prognostic model based on MCMGs in TCGA-LIHC

Among the MCMG-associated genes examined, twelve differentially expressed MCMGs were correlated with patient OS (*Figure 3A*, P<0.05). Using LASSO Cox regression analysis, six MCMGs (*ACADL*, *ACLY*, *TXNRD1*, *DTYMK*, *ACAT1*, and *FLAD1*) were further narrowed down as candidates (*Figure 3B*). The prognostic risk model incorporating these six MCMGs was developed, with the corresponding risk score calculated as follows: $expression_{ACADL} \times (-0.00225986735977285) + expression_{ACLY} \times (0.29204276361915) + expression_{TXNRD1} \times (0.1788365366618723) + expression_{DTYMK} \times (0.374908734507949) + expression_{ACAT1} \times (-0.260229157656772) + expression_{FLAD1} \times (0.0406045953218403)$. Patients with HCC were divided into high-risk and low-risk groups based on their median risk score. Analysis showed a higher mortality rate in the high-risk group (*Figure 3C*). The heatmap revealed significant down-regulation of *ACADL* and *ACAT1*, and up-regulation of *FLAD1*, *TXNRD1*, *DTYMK*, and *ACLY* in the high-risk group (*Figure 3D*). Survival analysis indicated a higher survival rate in the low-risk group (*Figure 3E*). The areas under the curve (AUC) for the 1-, 2-, 3-, 4-, and 5-year time points were 0.785, 0.752, 0.756, 0.774, and 0.759, respectively, as shown in the time-dependent ROC curve (*Figure 3F*). These findings indicated that the MCMGs model exhibits a notable predictive capability.

Verification of prognostic model of MCMGs

The ICGC and GSE14520 external validation datasets were categorized into high-risk and low-risk groups according to their risk scores that were calculated. Examination of risk distribution, survival status maps, and survival curves indicated significantly lower survival rates in the high-risk group compared to the low-risk group (*Figure 4A-4D*). Through time-dependent ROC curve analysis, the risk score model demonstrated high accuracy in predicting survival outcomes within the ICGC and GSE14520 validation
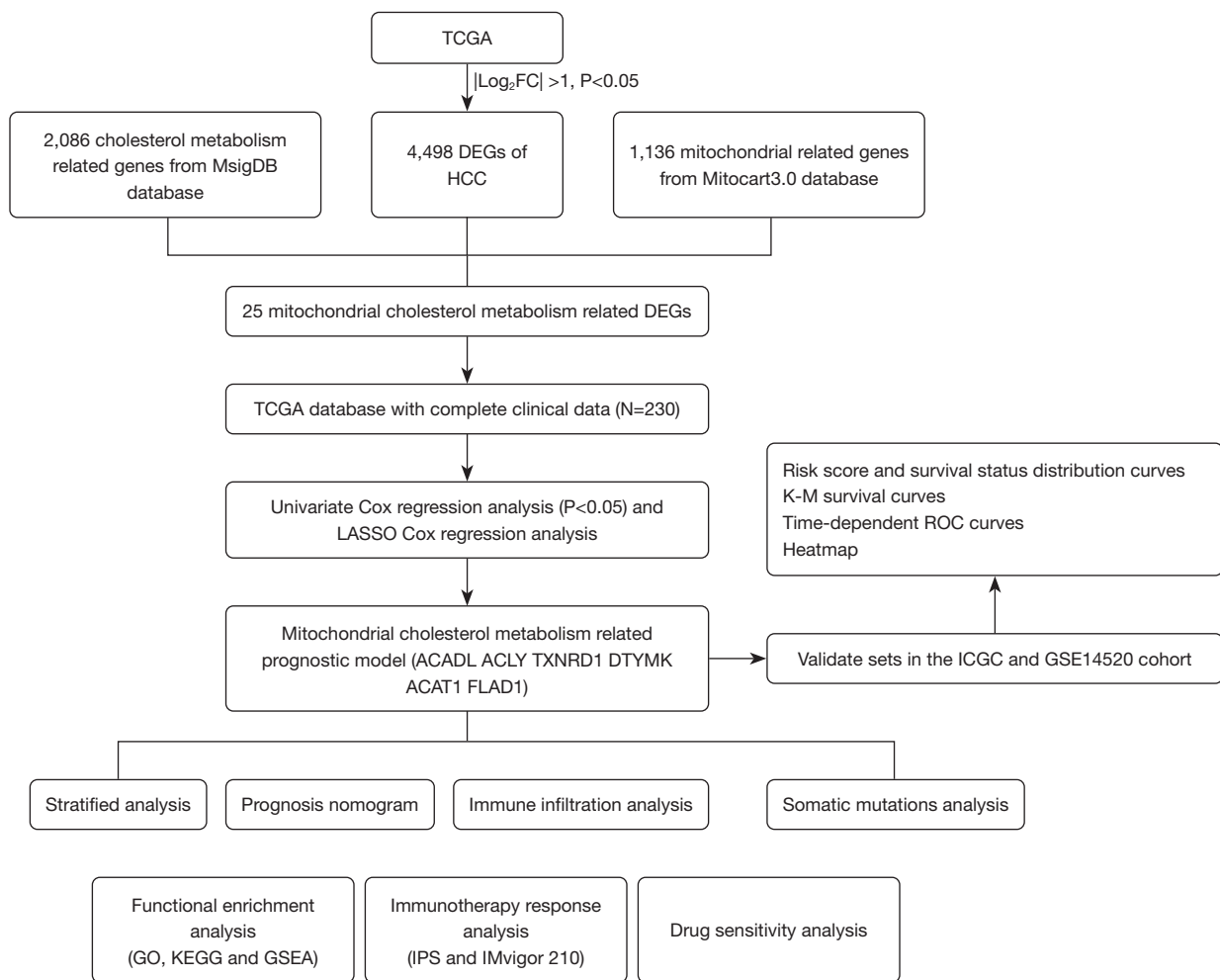
Figure 1 Flowchart for the model of MCMGs. TCGA, The Cancer Genome Atlas; FC, fold change; DEG, differentially expressed genes; HCC, hepatocellular carcinoma; MsigDB, Molecular Signatures Database; K-M, Kaplan-Meier; ROC, receiver operating characteristic; LASSO, least absolute shrinkage and selection operator; ICGC, International Cancer Genome Consortium; GO, Gene Ontology; KEGG, Kyoto Encyclopedia of Genes and Genomes; GSEA, Gene Set Enrichment Analysis; IPS, immunophenoscore; MCMG, mitochondrial cholesterol metabolism-related gene.

sets (*Figure 4E,4F*). Additionally, the heatmap analysis demonstrated a significant down-regulation of *ACADL* and *ACAT1* expression in the high-risk group, while *FLAD1*, *TXNRD1*, *DTYMK*, and *ACLY* expression showed a marked increase in the same group (*Figure 4G,4H*). These results indicated that the forecasting model exhibits a high level of accuracy.

Validation of expression levels of relevant prognostic genes based on MCMGs

The study utilized RT-qPCR to assess mRNA levels of

prognostic genes in HCC cells, revealing upregulation of *DTYMK*, *ACLY*, and *FLAD1*, and downregulation of *TXNRD1*, *ACAT1*, and *ACADL*. The results aligned with the histological patterns of gene expression (*Figure 5A-5F*).

Stratified analysis and establishment of MCMGs nomogram

To further validate the prediction power of the various clinical features, a stratified analysis was performed (*Figure 6A*). Patients were categorized by age (≤65 *vs.* >65 years), gender (female *vs.* male), grade (1–2 *vs.* 3–4),

6628

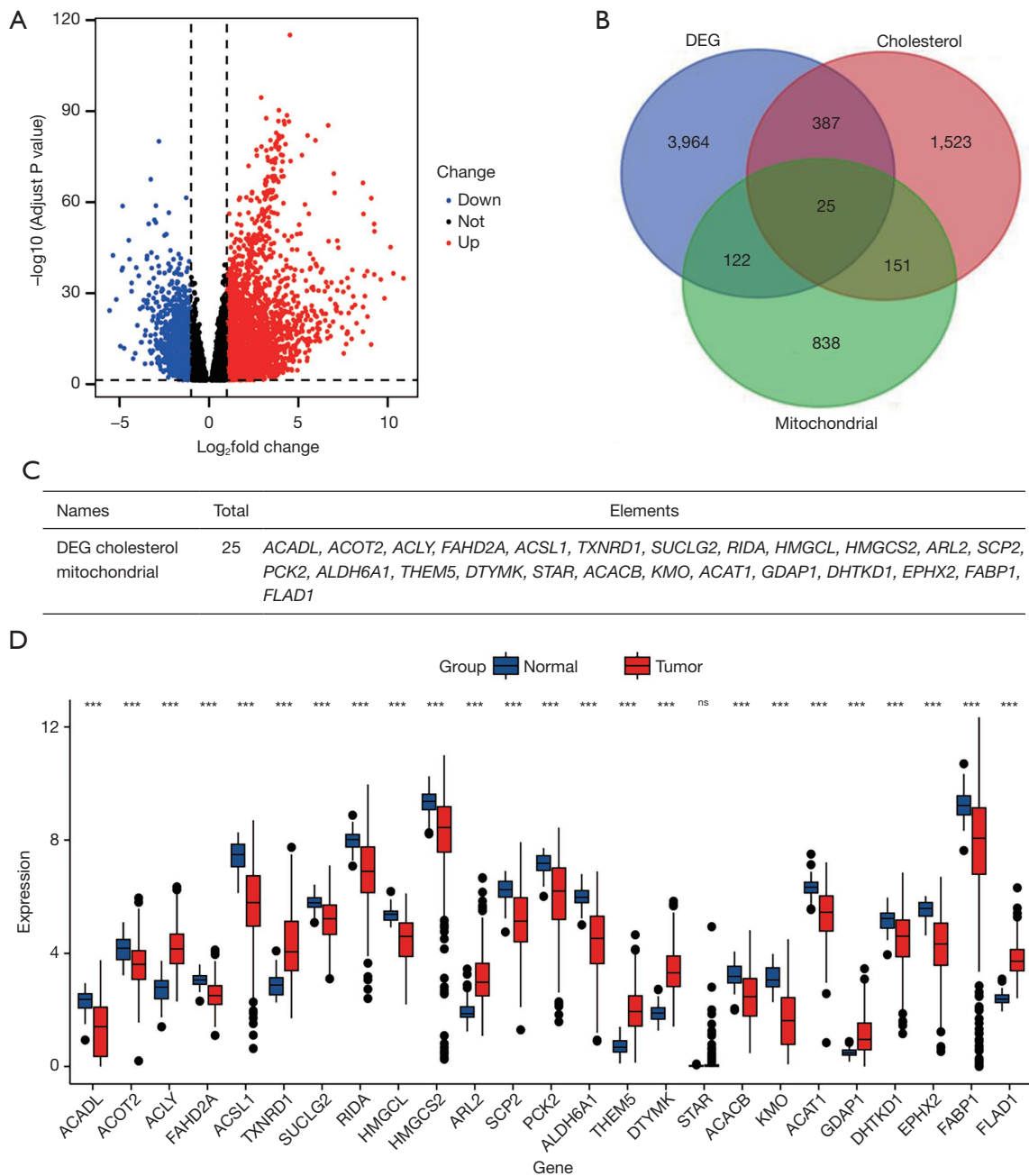Guo et al. Predictive MCMGs for HCC prognosis and treatment

Figure 2 Screening for mitochondrial cholesterol metabolism related DEGs. (A) Screening for DEGs in TCGA. (B) Venn chart of the mitochondrial cholesterol metabolism DEGs. (C) Number of mitochondrial cholesterol metabolism DEGs. (D) Expression of prognostically relevant MCMGs in normal and tumor samples. ns, not significant; ***, P<0.001. DEG, differentially expressed gene; TCGA, The Cancer Genome Atlas; MCMGs, mitochondrial cholesterol metabolism-related genes.
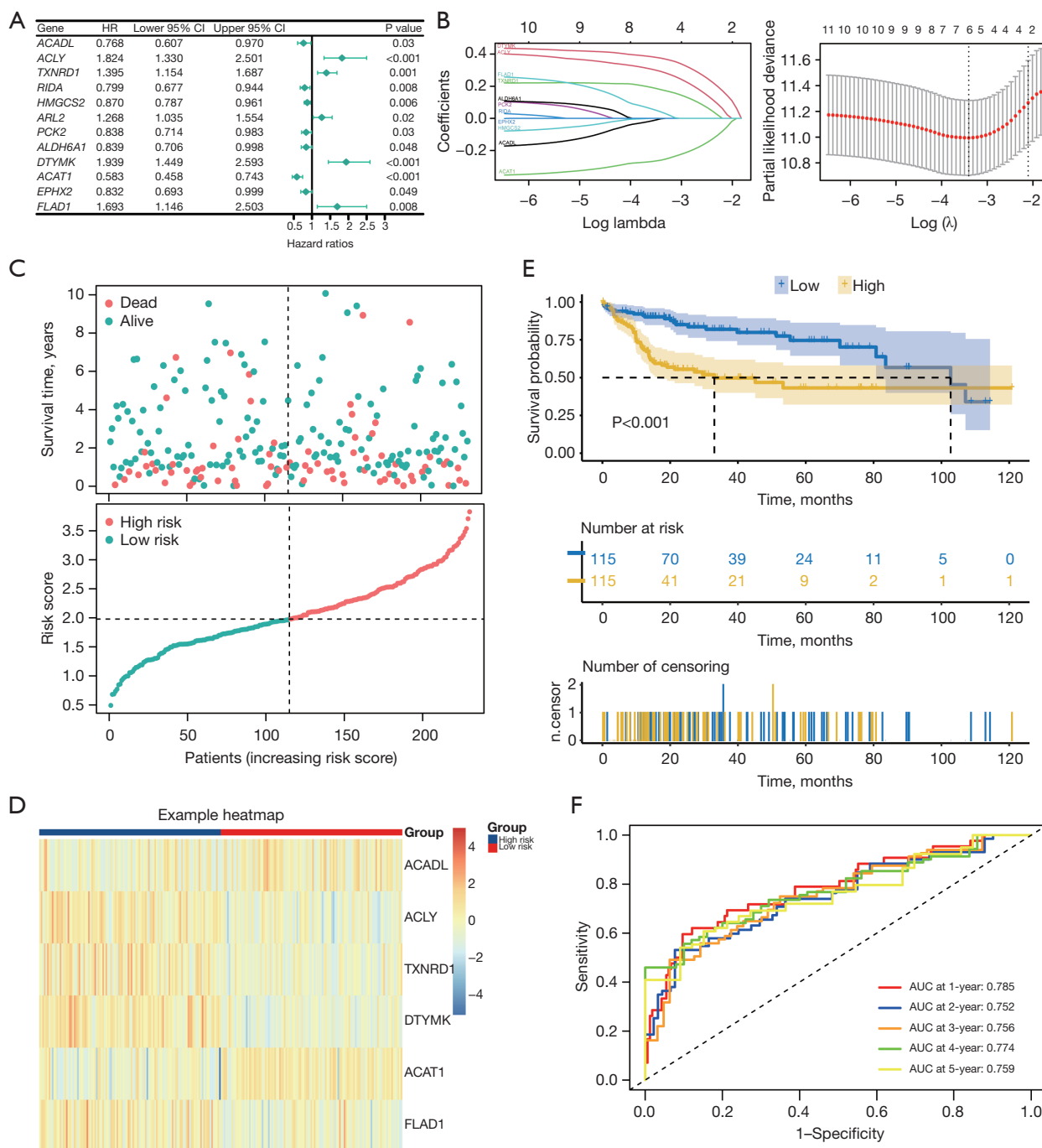
Figure 3 Construction of prognostic model. (A) Twelve MCMGs were screened based on univariate Cox regression analysis (P<0.1). (B) LASSO regression analysis identified six prognostically relevant MCMGs. (C) Risk score distribution, survival status in TCGA-LIHC cohort. (D) The six genes expression heatmaps in TCGA-LIHC cohort. (E) Kaplan-Meier survival analysis. (F) Time-dependent ROC curves. AUC, area under the curve; MCMGs, mitochondrial cholesterol metabolism-related genes; LASSO, least absolute shrinkage and selection operator; TCGA-LIHC, The Cancer Genome Atlas Liver Hepatocellular Carcinoma; ROC, receiver operating characteristic.
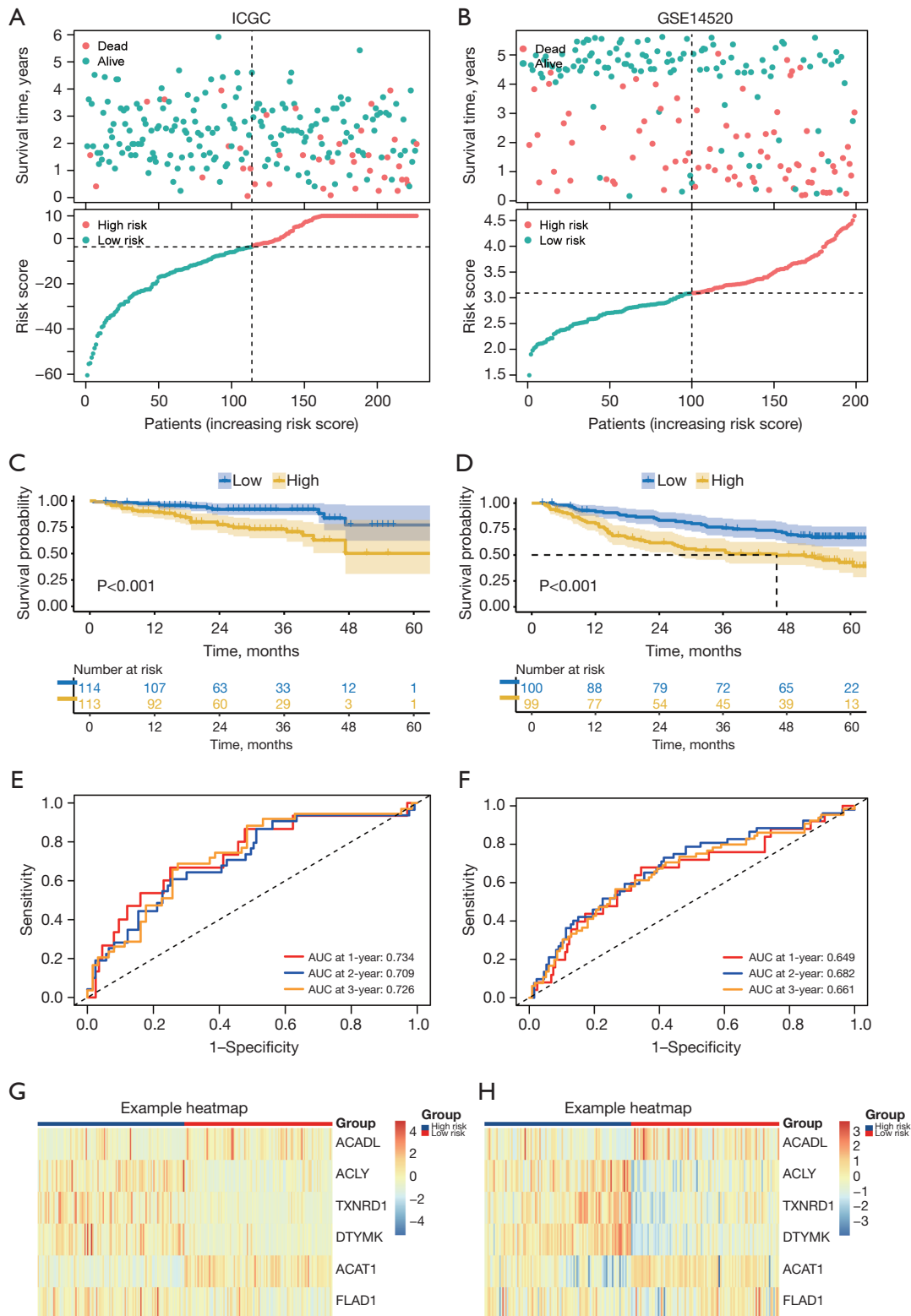
6630

Guo et al. Predictive MCMGs for HCC prognosis and treatment

Figure 4 Verification of prognostic models. (A,B) Risk score and survival status distribution in GSE14520 and ICGC. (C,D) Kaplan-Meier survival analysis. (E,F) Time-dependent ROC curves. (G,H) The six genes expression heatmaps in ICGC and GSE14520 cohort. ICGC, International Cancer Genome Consortium; AUC, area under the curve; ROC, receiver operating characteristic.
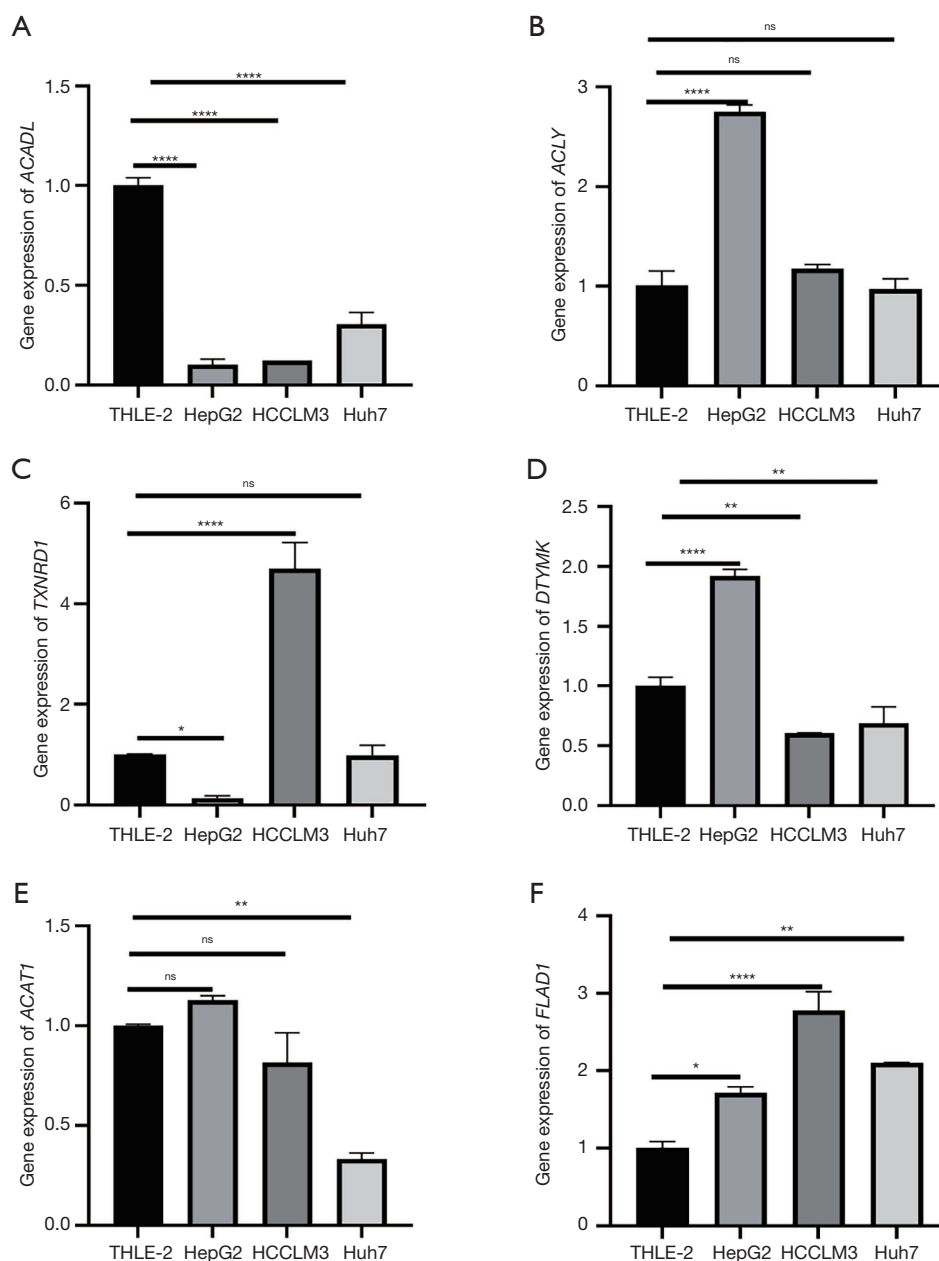
Figure 5 Expression levels of prognostic genes. (A-F) Expression levels of prognostic genes associated with MCMGs. ns, not significant; *, P<0.05; **, P<0.01; ****, P<0.0001. THLE-2, transformed human liver epithelial-2; HepG2, human liver cancer cell; HCCLM3, human highly metastatic liver cancer cell; Huh7, human liver cancer cell; MCMGs, mitochondrial cholesterol metabolism-related genes.

stage (I–II vs. III–IV), and T (1–2 vs. 3–4) (*Figure 6B*). Excluding gender, G1–2, M and N, the low-risk group demonstrated a higher survival rate than the high-risk group (*Figure 6C*). Univariate Cox analysis revealed that stage, T, M, and risk score were significantly associated with the prognosis of HCC patients. Furthermore, multivariate Cox analysis demonstrated that the risk score remains an independent predictor of prognosis in HCC patients after adjusting for other confounding factors (*Figure 7A,7B*). As shown by the result of multivariate Cox regression analysis, the risk score continued to be a reliable predictor of survival (*Figure 7B*). This risk score, along with stage, T, and M, contributed to the development of a nomogram predicting the survival probabilities at 1-, 2-, 3-, 4-, and 5-year
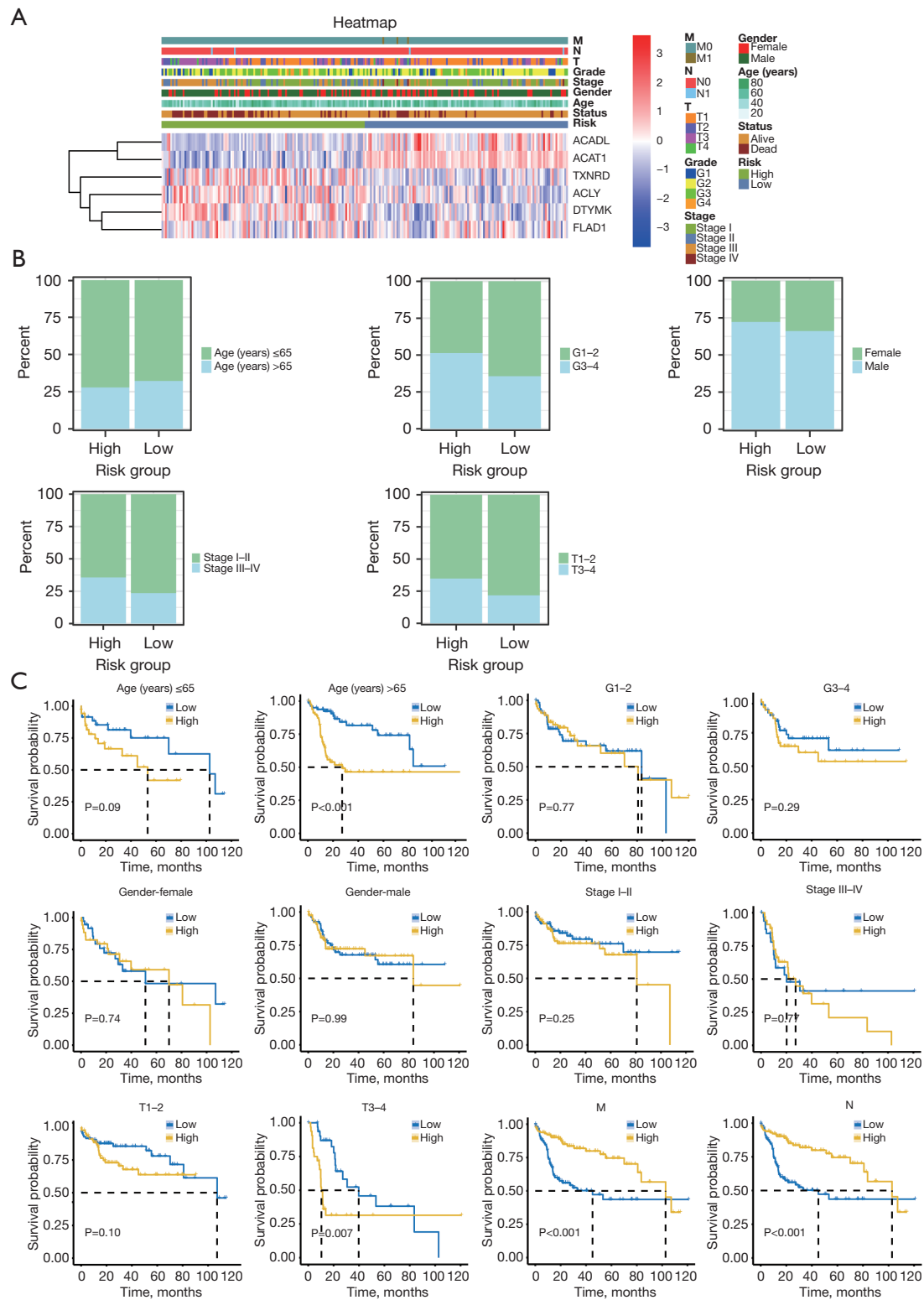
Figure 6 Prognostic modeling and clinicopathologic stratification of hepatocellular carcinoma patients. (A) Heatmap of prognostic modeling and clinicopathologic features. (B) Distribution of different clinicopathologic features in the high- and low-risk groups. (C) Survival of different clinicopathologic features in the high- and low-risk groups.
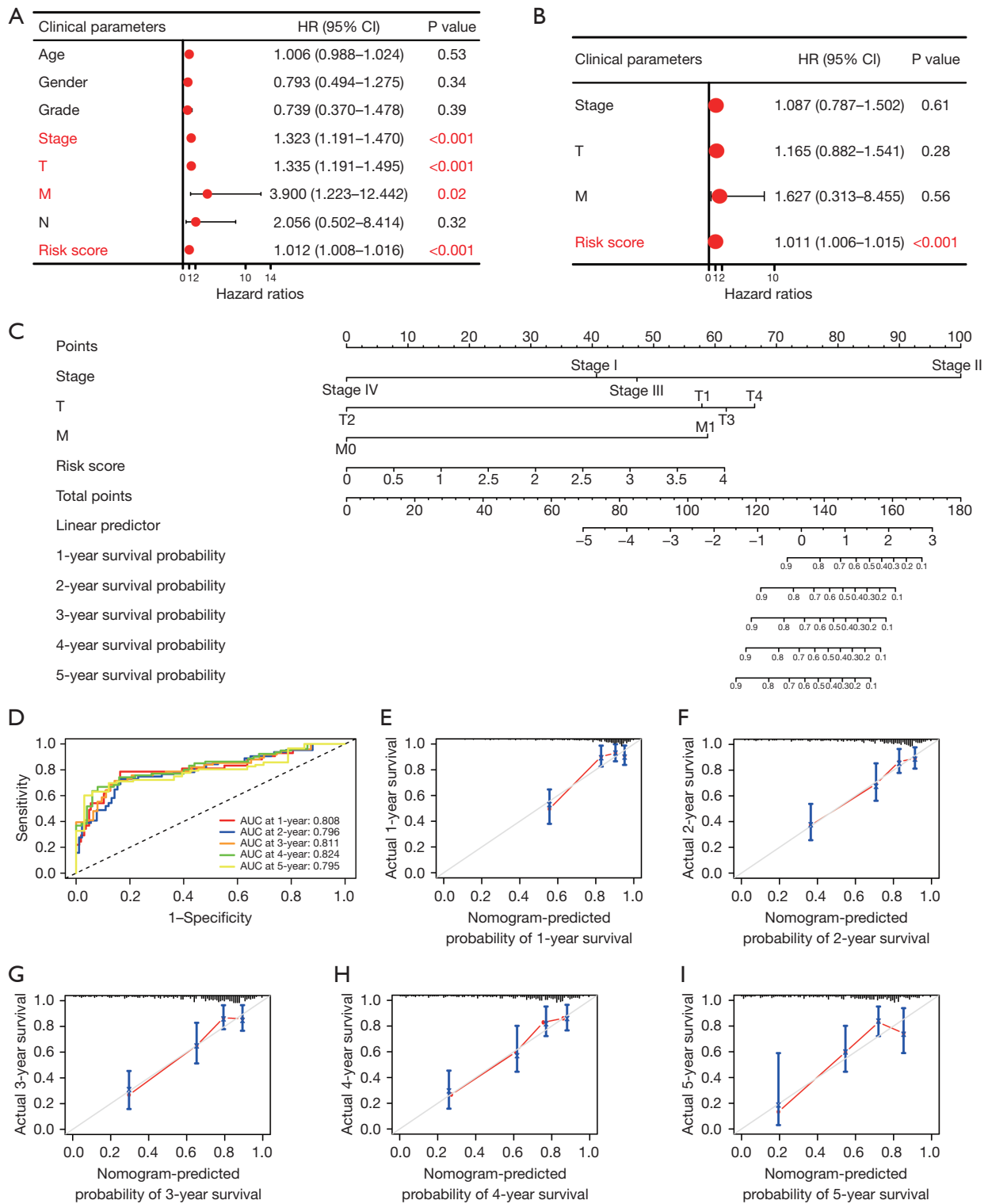
Figure 7 Construction and evaluation of a nomogram. (A) Clinical univariate analysis and (B) multivariate analysis of forest plots. (C) A nomogram plot. (D) Time-dependent ROC curves and (E-I) calibration curves for columnar plots predicting 1-, 2-, 3-, 4-, and 5-year overall survival rates. ROC, receiver operating characteristic; AUC, area under curve.

intervals for HCC patients (*Figure 7C*). The predictive accuracy was assessed by the area under the curve (AUC), which was found to be 0.808 at 1 year, 0.796 at 2 years, 0.811 at 3 years, 0.824 at 4 years, and 0.795 at 5 years (*Figure 7D*). The C-index value was 0.744, and the calibration curve demonstrated a good prediction accuracy (*Figure 7E-7I*). These findings implied that the nomogram has a higher predictive efficacy than a single risk score and provided a more precise estimation of patient survival probabilities.

Functional enrichment analysis and somatic mutation analysis

To investigate gene function and enrichment pathways among the high-risk and low-risk groups, a total of 1,304 DEGs ($|\log_2$ fold change$| > 1$) were identified. Functional enrichment analysis of these DEGs was conducted using Gene Ontology (GO), focusing on three main categories: biological processes (BPs), cellular components (CCs), and molecular functions (MFs). The analysis revealed significant enrichment in BPs associated with nuclear division, organelle fission, and chromosome segregation (*Figure 8A*). Pathway analysis from the KEGG revealed that processes associated with the cell cycle, complement and coagulation cascades, and retinol metabolism were significantly enriched (*Figure 8B*). The high-risk group showed enrichment in cell cycle, cell division, and chromosome processes (*Figure 8C*), whereas the low-risk group displayed enrichment in blood microparticle, cellular lipid metabolic process, and drug metabolic process (*Figure 8D*).

Prior research has demonstrated that tumor mutation burden (TMB) serves as a promising biomarker for forecasting tumor behavior and evaluating immunotherapy efficacy (25). To explore the relationship between risk score and mutations, somatic mutation analysis was utilized, leading to the identification of the top 20 genes with the highest mutation frequencies in both cohorts (*Figure 9A*). It was found that *TP53* had the highest mutation rate in the high-risk category (*Figure 9B*), whereas TTN was predominant in the low-risk group (*Figure 9C*). The high-risk group exhibited a significantly higher TMB value compared to the low-risk group (*Figure 9D*). Additionally, a significant correlation between the risk score and TMB was identified (*Figure 9E*).

Immune infiltration analysis

The impact of immune infiltration on high and low-risk groups was investigated using ssGSEA to compare the infiltration levels of 22 distinct immune cell types in each group. The results indicated significantly lower abundances of activated CD4 T cells (P<0.001), type 2 helper T cells (P<0.01), and neutrophils (P<0.01) in the high-risk group compared to the low-risk group (*Figure 10A*). Immune cell abundances corresponding to six prognostic genes were evaluated using the CIBERSORT algorithm, revealing a strong correlation (*Figure 10B*). The scatter plot indicated a positive correlation between the risk score and M0 macrophages, activated CD4$^+$ memory T cells, regulatory (Tregs) T cells, and follicular helper T cells (*Figure 10C*), as well as a negative correlation with resting mast cells, monocytes, and resting CD4 memory T cells (*Figure 10D*). Further analysis of immune checkpoint expression revealed significantly higher expression levels of *CD80*, *CTLA4*, *HAVCR2*, and *TNFRSF4* in the high-risk group compared to the low-risk group (P<0.001) (*Figure 10E*). The Estimation of STromal and Immune cells in MAlignant Tumours using Expression data (ESTIMATE) algorithm was employed to analyze the stromal score, immunological score, ESTIMATE score, and tumor purity in both groups (*Figure 10F*). It was observed that the low-risk group exhibited higher stromal scores, immunological scores, and ESTIMATE scores, whereas the high-risk group showed elevated levels of tumor purity. These findings indicated that there are discernible differences in the immune microenvironment between the low-risk and high-risk groups.

Immunotherapy efficacy prediction

To determine the potential utility of the MCMGs model as a prognostic tool for immunotherapy in patients with HCC, both IPS and iMvigor210 were utilized to assess the effectiveness of immunotherapy. Higher IPS scores were associated with a more favorable response to immune checkpoint inhibitor (ICI) therapy, encompassing treatments with programmed death 1 (PD-1) inhibitors and cytotoxic T lymphocyte-associated antigen-4 (CTLA4) inhibitors, and were categorized into four distinct groups: (I) ips_ctla4_neg_pd1_neg; (II) ips_ctla4_neg_pd1_pos; (III) ips_ctla4_pos_pd1_neg; (IV) ips_ctla4_pos_pd1_pos. Notably, individuals in the low-risk group demonstrated significantly elevated IPS compared to those in the high-risk group, indicating more favorable ICI treatment outcomes (*Figure 11A*). Further validation using the iMvigor210 data substantiates that the model could potentially improve

Figure 8 Functional enrichment analysis of differential genes between the high- and low-risk groups. (A) GO analysis. (B) KEGG analysis. (C,D) GSEA analysis in the high-risk group and low-risk group. GO, Gene Ontology; KEGG, Kyoto Encyclopedia of Genes and Genomes; GSEA, Gene Set Enrichment Analysis.

survival predictions for high-risk patients (*Figure 11B*) with a higher incidence of complete and partial responses (*Figure 11C,11D*). No significant differences were noted in the infiltration of immune cells or programmed death-ligand 1 (PD-L1) expression between the high and low-risk groups (*Figure 11E*); however, a greater percentage of tumor cells expressing PD-L1 was observed in the high-risk group (*Figure 11F*). These findings suggested that the model has the potential to identify individuals who may benefit from immunotherapy.

Drug sensitivity analysis

To further evaluate the clinical significance of the MCMGs model in treating HCC patients, the sensitivity analysis of chemotherapeutic drugs based on risk score was investigated. The chemotherapeutic medicines for HCC patients were identified in the Cancer Genome Project (CGP) database, and their effectiveness was evaluated in both high-risk and low-risk groups. It was found that individuals classified as high-risk exhibit heightened sensitivity to chemotherapeutic agents, including sorafenib,

6636

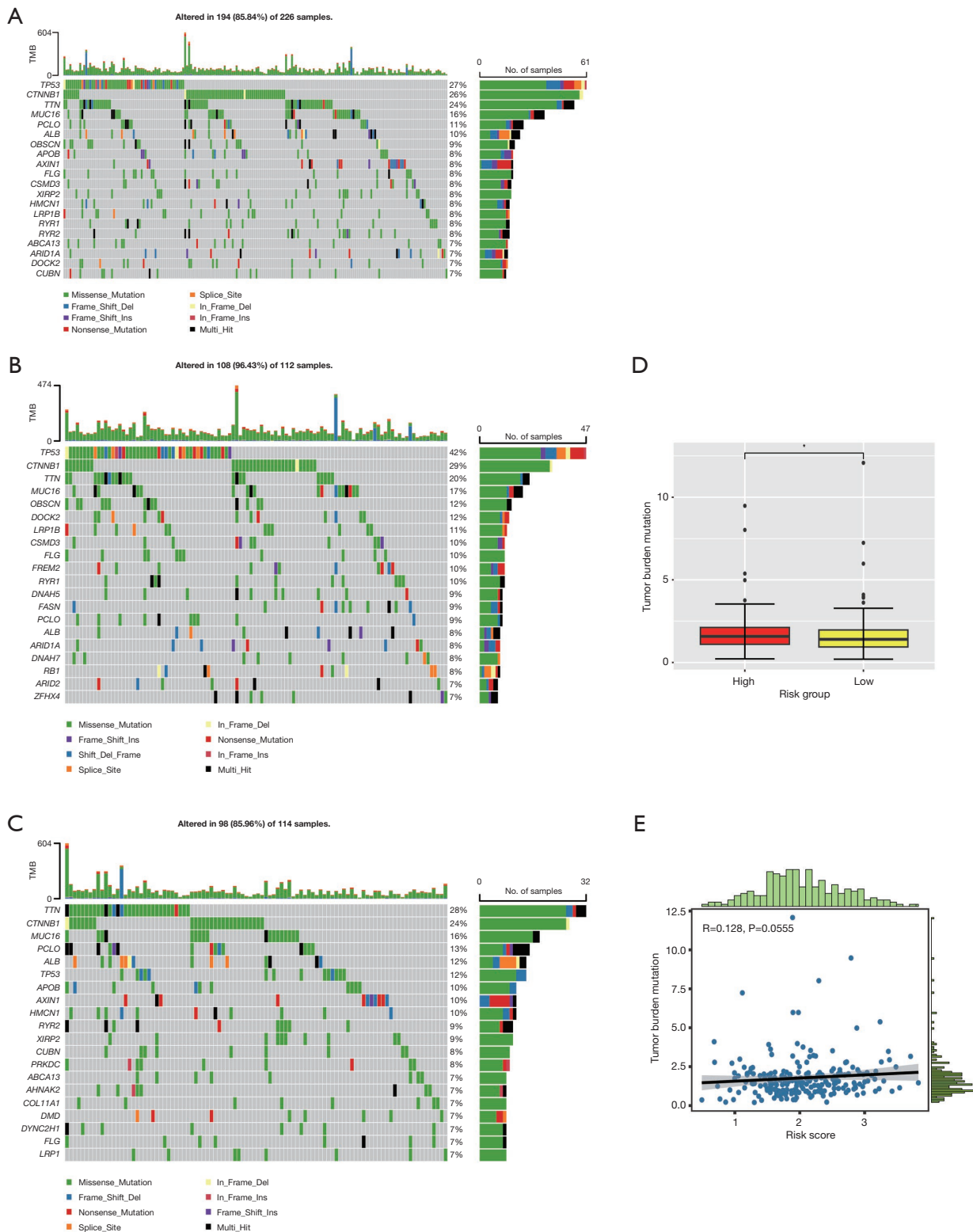Guo et al. Predictive MCMGs for HCC prognosis and treatment

Figure 9 Somatic mutation analysis. (A) Somatic mutation in 226 samples. (B) Somatic mutation waterfall plot in the high-risk group. (C) Somatic mutation waterfall plot in the low-risk group. (D) Box plot of tumor mutation load in the low and high-risk groups. (E) Scatterplot for analysis of correlation between tumor mutation load and risk score. *, P<0.05.
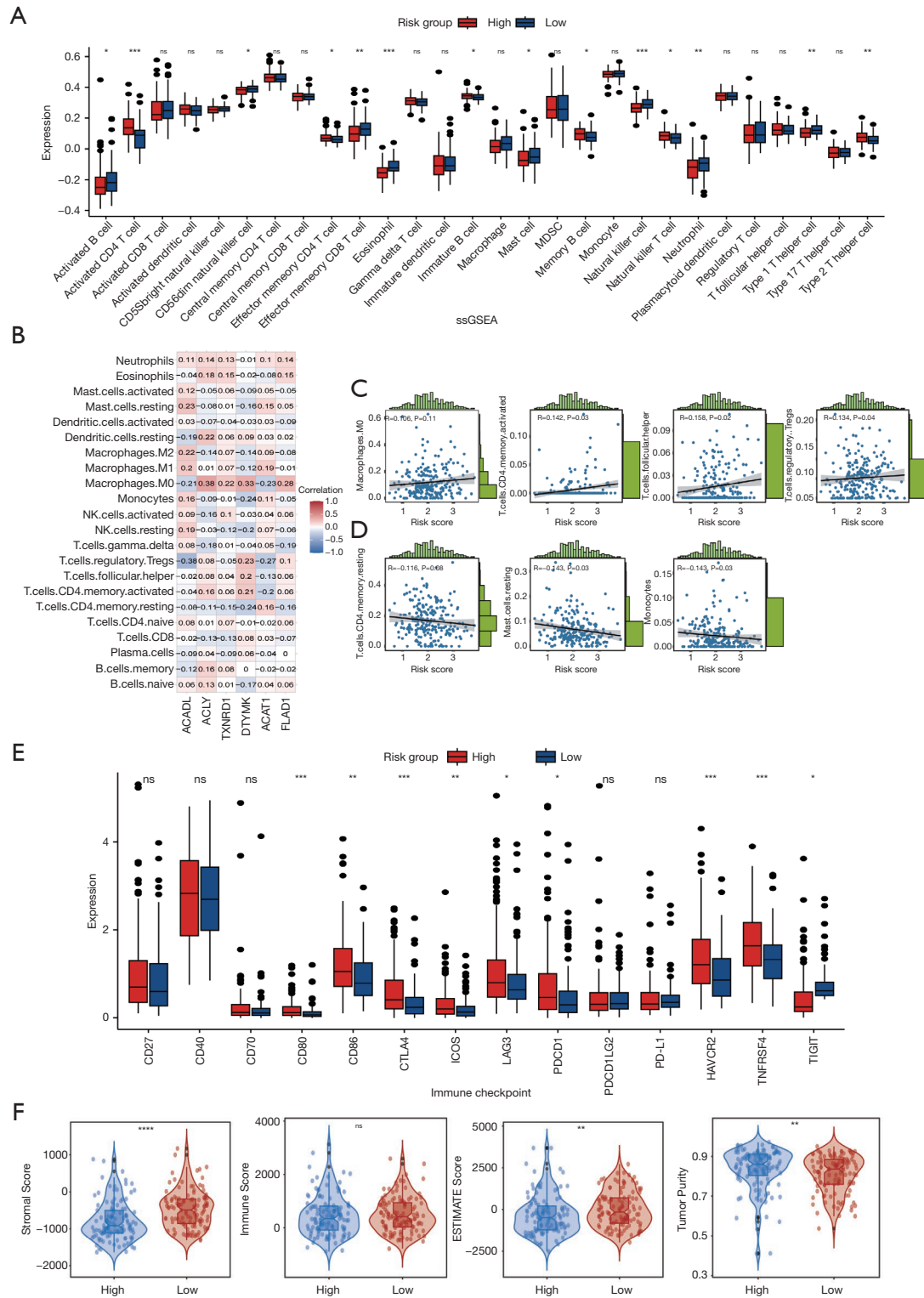
Figure 10 Immune infiltration analysis. (A) Comparison of infiltration with 28 immune cells in the high- and low-risk groups. (B) Heatmap for analysis of correlation of genes in prognostic tags with 22 immune cells. (C,D) Scatterplots for analysis of correlation between risk score and immune cells. (E) Comparison of expression levels of 14 immune checkpoints in the high- and low-risk groups. (F) Stromal score, immune score, estimation score, and tumor purity between the high- and low-risk groups. ns, not significant; *, P<0.05; **, P<0.01; ***, P<0.001; ***, P<0.0001.

6638

Guo et al. Predictive MCMGs for HCC prognosis and treatment
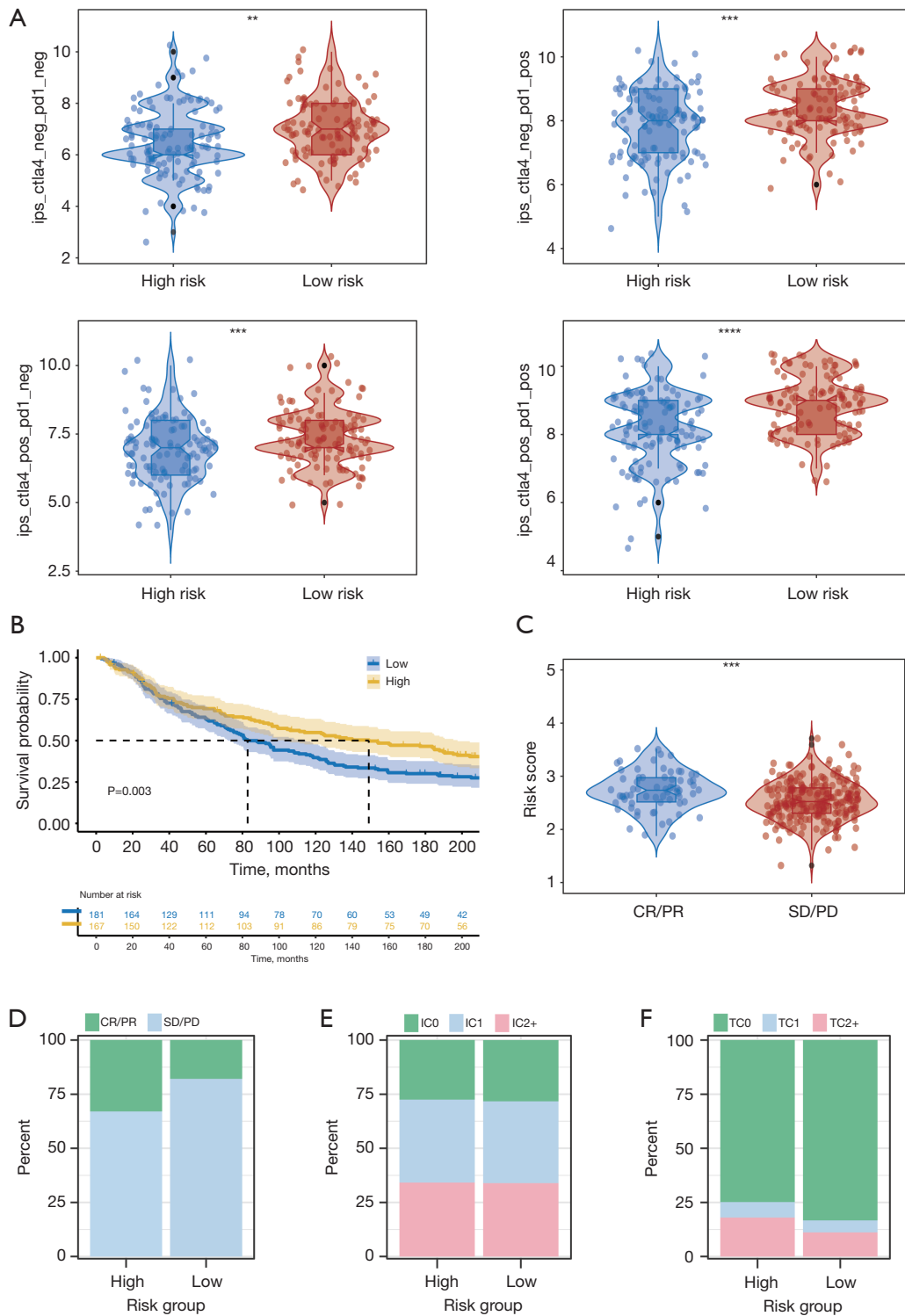
Figure 11 Immunotherapy sensitivity analysis. (A) Comparison of IPS scores between the high and low risk groups. (B) K-M survival analysis between the high and low risk groups in the iMvigor210 cohort. (C) Comparison of risk scores versus CR/PR and SD/PD in both groups. (D) Stacked plots of CR/PR and SD/PD in the high and low risk groups. (E,F) High and low risk IC0, IC1, IC2+ and TC0, TC1, TC2+ stacked plots in both groups. **, P<0.01; ***, P<0.001; ****, P<0.0001. IPS, immunophenoscore; CR/PR, complete response/partial response; SD/PD, stable disease/progressive disease.
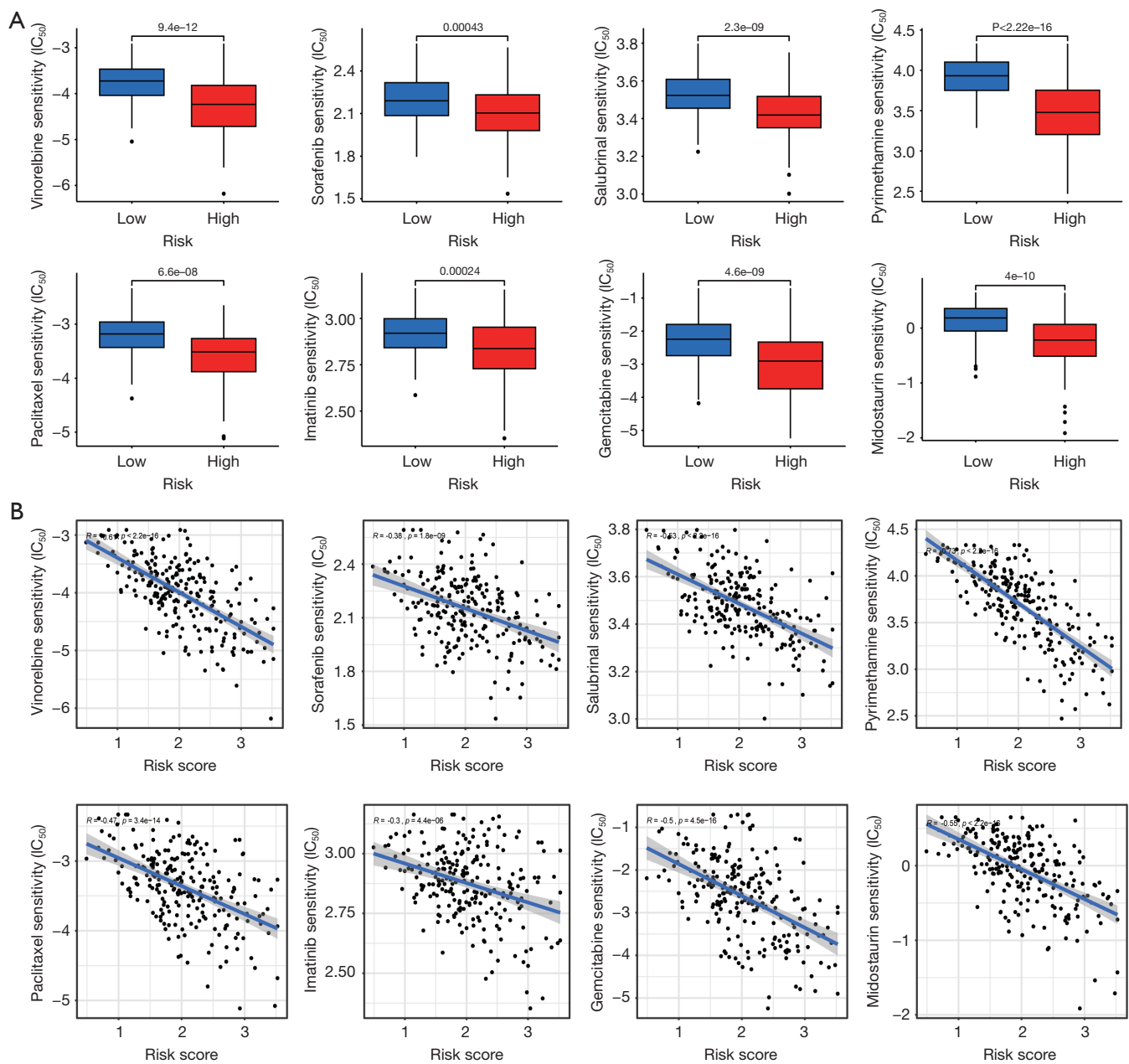
Figure 12 Drug sensitivity analysis. (A) Comparison of high and low risk groups for sensitivity to chemotherapeutic agents. (B) Correlation analysis between chemotherapeutic agents and risk score. IC$_{50}$, half maximal inhibitory concentration.

vinorelbine, salubrinal, pyrimethamine, paclitaxel, midostaurin, imatinib, and gemcitabine (*Figure 12A*). Similarly, the scatter plot illustrating the correlation analysis between risk score and drug sensitivity revealed that high-risk individuals had a higher susceptibility to these chemotherapeutic agents (*Figure 12B*). These results have shown that the model may inform clinical treatment and

drug resistance prevention in HCC patients.

Discussion

Cholesterol is vital not only for regulating the physical properties of cell membranes but also for modulating various signaling pathways (26-28). Although cholesterol is

6640

Guo et al. Predictive MCMGs for HCC prognosis and treatment

sparse in mitochondria, its limited availability substantially influences physiological processes (29). Proteins from the *STAR* family, such as *STARD1* and *MLN64* (also known as *StARD3*), play crucial roles in managing the movement of cholesterol within mitochondrial (11,30). An imbalance in cholesterol transport and metabolism can result in its accumulation, compromising the physical characteristics and fluidity of the mitochondrial membrane (31,32). Overexpression of *STARD1* may reroute cholesterol trafficking towards mitochondria for conversion into steroid hormones or bile acids, potentially overwhelming MCM and causing cholesterol accumulation in mitochondrial membranes (33). Research has shown that mitochondrial cholesterol levels in tumors from Buffalo rats with transplanted Morris hepatomas were 2- to 5-fold higher than those in mitochondria from the host liver, correlating with tumor growth rate and aggressiveness (34-37). Many solid tumors produce cholesterol-rich lipid rafts that facilitate tumor cell survival and proliferation by activating signaling pathways such as Akt (38-40). However, the specific mechanisms of MCM in HCC are not fully understood. This study aimed to establish signatures associated with MCM for clinical stratification, prognostic prediction, and immunotherapy analysis in HCC patients, introducing novel concepts for clinical management of HCC patients.

The study developed a six-gene predictive model comprising *ACADL*, *ACLY*, *TXNRD1*, *DTYMK*, *ACAT1*, and *FLAD3*. *ACADL* (long-chain Acyl-CoA dehydrogenase) plays a critical in the oxidation of long-chain fatty acyl-CoAs (41). Zhao *et al.* demonstrated that *ACADL* inhibits proliferation and growth of malignant tumor cells in human HCC by inducing cell cycle arrest, decreasing YAP nuclear localization, and inhibiting target gene transcription (42). Increased *ACADL* expression may enhance T-cell-driven cell death, suggesting its potential as a target for preventing immune evasion by cancer cells (41). *ACLY* (ATP citrate lyase) converts citrate to oxaloacetic acid (OAA) and acetyl-CoA, essential for membrane biogenesis, lipid synthesis, and histone acetylation in proliferating cancer cells (43). Inhibiting *ACLY* has been shown to increase PD-L1 immune checkpoint expression and disrupt T-cell activity, indicting complex interactions between metabolic pathways and immune regulation in cancer (44). *TXNRD1* (thioredoxin reductase 1) is found to be overexpressed in HCC clinical samples and cells, with high *TXNRD1* levels associated with advanced tumor stage and decreased survival, suggesting its potential as an adverse prognostic indicator (45). *TXNRD1*

is a limiting enzyme in the thioredoxin antioxidant pathway (46). *TXNRD1* prevents ferroptosis by alleviating lipid peroxidation, targeting its upstream regulators, such as miR21-3p, may induce ferroptosis in tumor cells and boost immunotherapy efficacy (47). *DTYMK* (deoxy thymidylate kinase) is linked to acid metabolism and cell cycle pathways and is associated with poor prognosis in HCC patients (48). *DTYMK* may enhance microsatellite instability (MSI) and TMB, potentially improving ICI efficacy (49). *ACAT1* (mitochondrial acetyl-CoA acetyltransferase 1) inhibition by arecoline hydrobromide (AH) disrupts tetrameric *ACAT1*, increasing pyruvate dehydrogenase complex (PDC) flow and oxidative phosphorylation while reducing cancer cell proliferation and tumor growth (50). Inhibition of *ACAT1* also enhances CD8$^+$ T-cell effector function (51). *FLAD1*, encoding flavin adenine dinucleotide synthetase (FADS), is widely expressed in human tissues and is associated with the prognosis and survival of malignant tumors due to its role in the oxidation-reduction chain (52). However, there is no evidence indicating a role for *FLAD1* in immunotherapy, which warrants further investigation. These results imply that the above six genes have a substantial role in the emergence of tumors. The importance of this characteristic was validated by creating a composite nomogram plot of this characteristic together with the clinical characteristics (T, age, and gender).

The tumor microenvironment (TME), consisting of immunological, stromal, and cancer cells, is crucial in tumor initiation, progression, metastasis, and therapeutic response (53-55). The research demonstrated that individuals in the low-risk group exhibited increased counts of eosinophils and natural killer cells, known for their antitumorigenic properties (56). Additionally, high blood cholesterol and cholesterol accumulation in natural killer (NK) cells facilitate lipid raft development in liver-tumor-bearing mouse models, highlighting the diverse roles of lipid metabolism in cancer (57-59). Furthermore, the connection between the TME and risk score were explored and discovered that they were strongly connected. One of the primary causes of carcinogenesis and a factor in the growth of neoantigens is the accumulation of somatic mutations. TMB serves as a prognostic biomarker for understanding tumor biology and immune responses (60,61). Significant differences in TMB were observed between high-risk and low-risk groups, with a positive correlation between risk score and TMB levels. *TP53*, a key tumor-suppressor gene, had the highest prevalence in the high-risk category. Mutations in *TP53* diminish its anticancer activity and

enhance the oncogenic properties of the mutant p53 protein (62). Malignancies with mutated p53 frequently exhibit poor prognosis, rapid tumor progression, and suboptimal responses to anticancer therapy (63,64). *TTN* exhibited the highest incidence of mutations within the low-risk category. Individuals with *TTN* mutations typically experience a more favorable prognosis, with these mutations predominantly occurring in solid tumors. Furthermore, *TTN* mutations are correlated with increased responsiveness to high TMB and ICIs (65).

The immune cells within the TME initially target and eliminate cancer cells but eventually, cancer cells evade immune detection and suppress cytotoxic functions through various mechanisms (66,67). The combination of ICIs with adoptive cell transfer (ACT) has improved outcomes for patients with metastatic or advanced cancers (68). Disrupting ICI pathways with monoclonal antibodies against CTLA-4 and PD-1 has become popular in immunotherapy (69). The study revealed that the low-risk group exhibited more resistance to ICIs, with complete and partial responses after immunotherapy more frequently observed in the high-risk group, suggesting the model usefulness as an immunotherapy indicator. Previous studies have suggested that cross-tumor data may predict immunotherapy effectiveness (70-72). Patients with cirrhosis generally exhibit poor tolerance to chemotherapy due to resistance and significant side effects (73,74). The finding indicated that different risk groups have different choices of chemotherapeutic agents, with the high-risk group having higher sensitivity to chemotherapeutic agents. This may help in selecting chemotherapeutic agents for HCC patients, although only a small proportion benefit from them (75), despite their long-term therapeutic success.

Conclusions

In conclusion, this study developed and validated a *MCMGs* model with a strong predictive power for survival times, immunotherapy response, and drug sensitivity in HCC patients. This model has been shown to correlate with the prognosis for HCC patients, and may provide clues to potential therapeutic targets. The present study has shown that this model has a promising application in immunotherapy and there was a significant difference in the sensitivity to chemotherapeutic agents between the high-risk and low-risk groups, which may be helpful for clinical treatment. Overall, the results provided a new perspectives and avenues for the management and treatment of HCC.

Footnote

Reporting Checklist: The authors have completed the TRIPOD reporting checklist. Available at https://tcr.amegroups.com/article/view/10.21037/tcr-24-1153/rc

Data Sharing Statement: Available at https://tcr.amegroups.com/article/view/10.21037/tcr-24-1153/dss

Peer Review File: Available at https://tcr.amegroups.com/article/view/10.21037/tcr-24-1153/prf

Conflicts of Interest: All authors have completed the ICMJE uniform disclosure form (available at https://tcr.amegroups.com/article/view/10.21037/tcr-24-1153/coif). The authors have no conflicts of interest to declare.

Ethical Statement: The authors are accountable for all aspects of the work in ensuring that questions related to the accuracy or integrity of any part of the work are appropriately investigated and resolved. The study was conducted in accordance with the Declaration of Helsinki (as revised in 2013).

6642

Guo et al. Predictive MCMGs for HCC prognosis and treatment

References

1. Siegel RL, Giaquinto AN, Jemal A. Cancer statistics, 2024. CA Cancer J Clin 2024;74:12-49.

2. Rumgay H, Arnold M, Ferlay J, et al. Global burden of primary liver cancer in 2020 and predictions to 2040. J Hepatol 2022;77:1598-606.

3. Zhong JH, Peng NF, You XM, et al. Tumor stage and primary treatment of hepatocellular carcinoma at a large tertiary hospital in China: A real-world study. Oncotarget 2017;8:18296-302.

4. Suresh D, Srinivas AN, Prashant A, et al. Therapeutic options in hepatocellular carcinoma: a comprehensive review. Clin Exp Med 2023;23:1901-16.

5. Brown ZJ, Tsilimigras DI, Ruff SM, et al. Management of Hepatocellular Carcinoma: A Review. JAMA Surg 2023;158:410-20.

6. Xie DY, Zhu K, Ren ZG, et al. A review of 2022 Chinese clinical guidelines on the management of hepatocellular carcinoma: updates and insights. Hepatobiliary Surg Nutr 2023;12:216-28.

7. Zhang T, Nie Y, Gu J, et al. Identification of Mitochondrial-Related Prognostic Biomarkers Associated With Primary Bile Acid Biosynthesis and Tumor Microenvironment of Hepatocellular Carcinoma. Front Oncol 2021;11:587479.

8. Liu X, Lv M, Zhang W, et al. Dysregulation of cholesterol metabolism in cancer progression. Oncogene 2023;42:3289-302.

9. Wang X, Shi J, Huang M, et al. TUBB2B facilitates progression of hepatocellular carcinoma by regulating cholesterol metabolism through targeting HNF4A/CYP27A1. Cell Death Dis 2023;14:179.

10. Feng XC, Liu FC, Chen WY, et al. Lipid metabolism of hepatocellular carcinoma impacts targeted therapy and immunotherapy. World J Gastrointest Oncol 2023;15:617-31.

11. Goicoechea L, Conde de la Rosa L, Torres S, et al. Mitochondrial cholesterol: Metabolism and impact on redox biology and disease. Redox Biol 2023;61:102643.

12. Ye W, Shi Z, Zhou Y, et al. Autophagy-Related Signatures as Prognostic Indicators for Hepatocellular Carcinoma. Front Oncol 2022;12:654449.

13. Lei L, Li N, Yuan P, et al. A new risk model based on a 11-m(6)A-related lncRNA signature for predicting prognosis and monitoring immunotherapy for gastric cancer. BMC Cancer 2022;22:365.

14. Liu P, Wei J, Mao F, et al. Establishment of a Prognostic Model for Hepatocellular Carcinoma Based on Endoplasmic Reticulum Stress-Related Gene Analysis. Front Oncol 2021;11:641487.

15. Zhang Y, Zhang K, Jia H, et al. IVIM-DWI and MRI-based radiomics in cervical cancer: Prediction of concurrent chemoradiotherapy sensitivity in combination with clinical prognostic factors. Magn Reson Imaging 2022;91:37-44.

16. Xu H, Xing Z, Wang J, et al. Development and external validation of nomograms for predicting disease-free survival and overall survival in patients with cT1-ccRCC after partial nephrectomy: a multicenter retrospective study. Ann Surg Oncol 2024;31:5827-38.

17. Wu T, Hu E, Xu S, et al. clusterProfiler 4.0: A universal enrichment tool for interpreting omics data. Innovation (Camb) 2021;2:100141.

18. Wang B, van der Kloet F, Kes MBMJ, et al. Improving gene set enrichment analysis (GSEA) by using regulation directionality. Microbiol Spectr 2024;12:e0345623.

19. Li B, Chen X, Xian H, et al. Gene mutation analysis of oral submucous fibrosis cancerization in Hainan Island. PeerJ 2023;11:e16392.

20. Zhu J, Wang J, Wang T, et al. Identification of molecular subtypes, risk signature, and immune landscape mediated by necroptosis-related genes in non-small cell lung cancer. Front Oncol 2022;12:955186.

21. Sousa Â, Soares CP, Chin CM, et al. Editorial: Epigenetic therapy against cancer: toward new molecular targets and technologies. Front Cell Dev Biol 2023;11:1218986.

22. Chang W, Li H, Zhong L, et al. Development of a copper metabolism-related gene signature in lung adenocarcinoma. Front Immunol 2022;13:1040668.

23. Yan C, Niu Y, Ma L, et al. System analysis based on the cuproptosis-related genes identifies LIPT1 as a novel therapy target for liver hepatocellular carcinoma. J Transl Med 2022;20:452.

24. Liu J, Shen H, Gu W, et al. Prediction of prognosis, immunogenicity and efficacy of immunotherapy based on glutamine metabolism in lung adenocarcinoma. Front Immunol 2022;13:960738.

25. Russano M, La Cava G, Cortellini A, et al. Immunotherapy for Metastatic Non-Small Cell Lung Cancer: Therapeutic Advances and Biomarkers. Curr Oncol 2023;30:2366-87.

26. Chen F, Lu Y, Lin J, et al. Cholesterol Metabolism in Cancer and Cell Death. Antioxid Redox Signal 2023;39:102-40.

27. Kumar R, Chhillar N, Gupta DS, et al. Cholesterol Homeostasis, Mechanisms of Molecular Pathways, and

Cardiac Health: A Current Outlook. Curr Probl Cardiol 2024;49:102081.

28. Paukner K, Králová Lesná I, Poledne R. Cholesterol in the Cell Membrane-An Emerging Player in Atherogenesis. Int J Mol Sci 2022;23:533.

29. Braczko A, Harasim G, Kawecka A, et al. Blocking cholesterol formation and turnover improves cellular and mitochondria function in murine heart microvascular endothelial cells and cardiomyocytes. Front Physiol 2023;14:1216267.

30. Altinkilic EM, Augsburger P, Pandey AV, et al. Clinical spectrum of human STAR variants and their genotype-phenotype correlation. J Endocrinol 2024;262:e240078.

31. Bassi G, Sidhu SK, Mishra S. The Expanding Role of Mitochondria, Autophagy and Lipophagy in Steroidogenesis. Cells 2021;10:1851.

32. Da Dalt L, Cabodevilla AG, Goldberg IJ, et al. Cardiac lipid metabolism, mitochondrial function, and heart failure. Cardiovasc Res 2023;119:1905-14.

33. Kakiyama G, Rodriguez-Agudo D, Pandak WM. Mitochondrial Cholesterol Metabolites in a Bile Acid Synthetic Pathway Drive Nonalcoholic Fatty Liver Disease: A Revised "Two-Hit" Hypothesis. Cells 2023;12:1434.

34. Feo F, Canuto RA, Bertone G, et al. Cholesterol and phospholipid composition of mitochondria and microsomes isolated from morris hepatoma 5123 and rat liver. FEBS Lett 1973;33:229-32.

35. Crain RC, Clark RW, Harvey BE. Role of lipid transfer proteins in the abnormal lipid content of Morris hepatoma mitochondria and microsomes. Cancer Res 1983;43:3197-202.

36. Campbell AM, Capuano A, Chan SH. A cholesterol-binding and transporting protein from rat liver mitochondria. Biochim Biophys Acta 2002;1567:123-32.

37. Feo F, Canuto RA, Garcea R, et al. Effect of cholesterol content on some physical and functional properties of mitochondria isolated from adult rat liver, fetal liver, cholesterol-enriched liver and hepatomas AH-130, 3924A and 5123. Biochim Biophys Acta 1975;413:116-34.

38. Gupta A, Das D, Taneja R. Targeting Dysregulated Lipid Metabolism in Cancer with Pharmacological Inhibitors. Cancers (Basel) 2024;16:1313.

39. Isik OA, Cizmecioglu O. Rafting on the Plasma Membrane: Lipid Rafts in Signaling and Disease. Adv Exp Med Biol 2023;1436:87-108.

40. Wu H, Wu X, Zhao M, et al. Regulating Cholesterol in Tumorigenesis: A Novel Paradigm for Tumor Nanotherapeutics. Int J Nanomedicine 2024;19:1055-76.

41. Li L, Wang LL, Wang TL, et al. ACADL suppresses PD-L1 expression to prevent cancer immune evasion by targeting Hippo/YAP signaling in lung adenocarcinoma. Med Oncol 2023;40:118.

42. Zhao X, Qin W, Jiang Y, et al. ACADL plays a tumor-suppressor role by targeting Hippo/YAP signaling in hepatocellular carcinoma. NPJ Precis Oncol 2020;4:7.

43. Kuna RS, Kumar A, Wessendorf-Rodriguez KA, et al. Inter-organelle cross-talk supports acetyl-coenzyme A homeostasis and lipogenesis under metabolic stress. Sci Adv 2023;9:eadf0138.

44. Xiang W, Lv H, Xing F, et al. Inhibition of ACLY overcomes cancer immunotherapy resistance via polyunsaturated fatty acids peroxidation and cGAS-STING activation. Sci Adv 2023;9:eadi2465.

45. Huang WY, Liao ZB, Zhang JC, et al. USF2-mediated upregulation of TXNRD1 contributes to hepatocellular carcinoma progression by activating Akt/mTOR signaling. Cell Death Dis 2022;13:917.

46. Yang R, Sun S, Zhang Q, et al. Pharmacological Inhibition of TXNRD1 by a Small Molecule Flavonoid Butein Overcomes Cisplatin Resistance in Lung Cancer Cells. Biol Trace Elem Res 2024. [Epub ahead of print]. doi: 10.1007/s12011-024-04331-0.

47. Guo W, Wu Z, Chen J, et al. Nanoparticle delivery of miR-21-3p sensitizes melanoma to anti-PD-1 immunotherapy by promoting ferroptosis. J Immunother Cancer 2022;10:e004381.

48. Guo Y, Luo W, Huang S, et al. DTYMK Expression Predicts Prognosis and Chemotherapeutic Response and Correlates with Immune Infiltration in Hepatocellular Carcinoma. J Hepatocell Carcinoma 2021;8:871-85.

49. Zhang Y, Wang H, Liu Y, et al. Comprehensive analysis of DTYMK in pan-cancer and verification in lung adenocarcinoma. Biosci Rep 2022;42:BSR20221170.

50. Fan J, Lin R, Xia S, et al. Tetrameric Acetyl-CoA Acetyltransferase 1 Is Important for Tumor Growth. Mol Cell 2016;64:859-74.

51. Su Q, Yao J, Farooq MA, et al. Modulating Cholesterol Metabolism via ACAT1 Knockdown Enhances Anti-B-Cell Lymphoma Activities of CD19-Specific Chimeric Antigen Receptor T Cells by Improving the Cell Activation and Proliferation. Cells 2024;13:555.

52. Hu P, Pan Y, Wang C, et al. FLAD1 is up-regulated in Gastric Cancer and is a potential prediction of prognosis. Int J Med Sci 2020;17:1763-72.

53. Xiao Y, Yu D. Tumor microenvironment as a therapeutic

target in cancer. Pharmacol Ther 2021;221:107753.

54. de Visser KE, Joyce JA. The evolving tumor microenvironment: From cancer initiation to metastatic outgrowth. Cancer Cell 2023;41:374-403.

55. Babar Q, Saeed A, Tabish TA, et al. Targeting the tumor microenvironment: Potential strategy for cancer therapeutics. Biochim Biophys Acta Mol Basis Dis 2023;1869:166746.

56. Grisaru-Tal S, Itan M, Klion AD, et al. A new dawn for eosinophils in the tumour microenvironment. Nat Rev Cancer 2020;20:594-607.

57. Wu SY, Fu T, Jiang YZ, et al. Natural killer cells in cancer biology and therapy. Mol Cancer 2020;19:120.

58. Elaraby E, Malek AI, Abdullah HW, et al. Natural Killer Cell Dysfunction in Obese Patients with Breast Cancer: A Review of a Triad and Its Implications. J Immunol Res 2021;2021:9972927.

59. Giordo R, Wehbe Z, Paliogiannis P, et al. Nano-targeting vascular remodeling in cancer: Recent developments and future directions. Semin Cancer Biol 2022;86:784-804.

60. Wang T, Dai L, Shen S, et al. Comprehensive molecular analyses of a macrophage-related gene signature with regard to prognosis, immune features, and biomarkers for immunotherapy in hepatocellular carcinoma based on WGCNA and the LASSO algorithm. Front Immunol 2022;13:843408.

61. Moeckel C, Bakhl K, Georgakopoulos-Soares I, et al. The efficacy of tumor mutation burden as a biomarker of response to immune checkpoint inhibitors. Int J Mol Sci 2023;24:6710.

62. Pavlidis ET, Sapalidis KG, Pavlidis TE. Modern aspects of the management of pancreatic intraductal papillary mucinous neoplasms: a narrative review. Rom J Morphol Embryol 2022;63:491-502.

63. Hu J, Cao J, Topatana W, et al. Targeting mutant p53 for cancer therapy: direct and indirect strategies. J Hematol Oncol 2021;14:157.

64. Kwok M, Agathanggelou A, Davies N, et al. Targeting the p53 Pathway in CLL: State of the Art and Future

Perspectives. Cancers (Basel) 2021;13:4681.

65. Ahmed J, Das B, Shin S, et al. Challenges and Future Directions in the Management of Tumor Mutational Burden-High (TMB-H) Advanced Solid Malignancies. Cancers (Basel) 2023;15:5841.

66. Zhu YH, Zheng JH, Jia QY, et al. Immunosuppression, immune escape, and immunotherapy in pancreatic cancer: focused on the tumor microenvironment. Cell Oncol (Dordr) 2023;46:17-48.

67. Donne R, Lujambio A. The liver cancer immune microenvironment: Therapeutic implications for hepatocellular carcinoma. Hepatology 2023;77:1773-96.

68. Carlino MS, Larkin J, Long GV. Immune checkpoint inhibitors in melanoma. Lancet 2021;398:1002-14.

69. Oura K, Morishita A, Tani J, et al. Tumor Immune Microenvironment and Immunosuppressive Therapy in Hepatocellular Carcinoma: A Review. Int J Mol Sci 2021;22:5801.

70. Jiang Q, Chen L, Chen H, et al. Integrated Analysis of Stemness-Related LncRNAs Helps Predict the Immunotherapy Responsiveness of Gastric Cancer Patients. Front Cell Dev Biol 2021;9:739509.

71. Zheng H, Liu H, Li H, et al. Characterization of stem cell landscape and identification of stemness-relevant prognostic gene signature to aid immunotherapy in colorectal cancer. Stem Cell Res Ther 2022;13:244.

72. Li S, Chen P, Cheng B, et al. Pyroptosis predicts immunotherapy outcomes across multiple cancer types. Clin Immunol 2022;245:109163.

73. Singh AK, Singh SV, Kumar R, et al. Current therapeutic modalities and chemopreventive role of natural products in liver cancer: Progress and promise. World J Hepatol 2023;15:1-18.

74. Huang PS, Wang LY, Wang YW, et al. Evaluation and Application of Drug Resistance by Biomarkers in the Clinical Treatment of Liver Cancer. Cells 2023;12:869.

75. Zhang Y, Zhang Z. The history and advances in cancer immunotherapy: understanding the characteristics of tumor-infiltrating immune cells and their therapeutic implications. Cell Mol Immunol 2020;17:807-21.